Synoptic-Scale Weather Systems Observed during the FROST Project via Scatterometer Winds

GARETH J. MARSHALL AND JOHN TURNER

British Antarctic Survey, Natural Environment Research Council, Cambridge, United Kingdom

(Manuscript received 13 March 1998, in final form 25 March 1999)

ABSTRACT

Using data obtained during January 1995—the third of three special observing periods associated with the Antarctic First Regional Observing Study of the Troposphere project—over a sector of the Southern Ocean (SO), this study investigates the capabilities of European Remote Sensing satellite (ERS) scatterometer winds to portray accurately synoptic-scale weather systems and comments upon their potential contribution to the forecasting process in this region.

A sample population of cyclones was defined using satellite imagery and analyzed charts. The scatterometer successfully ''captured'' more than 60% of these systems that were existent over the open ocean. For manual analyses, the wind vectors proved extremely good for locating the positions of fronts, apparent as a marked turning in the wind direction, which coincided closely with frontal bands observed in contemporaneous satellite imagery. In most cases the wind vectors were also able to locate cyclone centers: their superior spatial resolution as compared with numerical analysis schemes revealed significant positional errors in the latter. This study demonstrates that typically each cyclone was captured twice by a scatterometer swath: such multitemporal data can provide information on the development of a system through changes in the strength of its associated winds.

Those 40% of systems that were not captured generally had a duration of less than a day and in that time were never encompassed by the scatterometer swath, a limiting factor in the instrument's effectiveness, as noted by other studies. However, this study reveals that the most significant problem in high southern latitudes appears to be missing data resulting from the use of the operationally mutually exclusive synthetic aperture radar instrument over coastal Antarctica. Additional limitations of scatterometer data for observing synoptic-scale systems are shown to be the maximum and minimum restrictions on the range of wind speeds that can be successfully derived and the granularity problems that are still existent in some ERS data. Nonetheless, scatterometer data have the potential to provide extremely important information for the forecasting process over the data-sparse SO, with the near-surface winds able to give an accurate reflection of the degree of activity of a weather system.

1. Introduction

Routine observations over the sea obtained by conventional methods (buoys and ships) lack the necessary spatial resolution to enable the accurate location of cyclone centers in numerical weather prediction (NWP) models and also tend to be concentrated in particular regions (e.g., shipping lanes). However, spaceborne radar scatterometer instruments can provide high-quality global coverage of surface wind vectors over the world's oceans. The potential utility of scatterometer winds to the meteorological community was first demonstrated by the Seasat mission of 1978. Overviews of the wind field data obtained from this sensor and its application to synoptic-scale weather systems are given by Guymer (1983) and Katsaros and Brown (1991). Levy and Brown (1991) presented detailed case studies of systems in the midlatitudes of the Southern Hemisphere (SH). They showed that the higher spatial resolution of the scatterometer data versus NWP analyses resulted in more accurate, sharper pressure gradients and deeper low pressure centers in the former using pressure fields derived from a planetary boundary layer model. However, Ingleby and Bromley (1991) revealed that while the assimilation of Seasat winds into the U.K. Meteorological Office (UKMO) forecast model resulted in the largest global pressure differences from a control run (without the winds) being observed in the data-sparse SH, such deviations were not necessarily beneficial to forecast accuracy.

More recently (since August 1991) such an instrument has been operational at C band (5.3 GHz) aboard the European Remote Sensing satellite (ERS) series (*ERS-1* and *-2*) and the National Aeronautics and Space Administration scatterometer operated briefly in 1997–98 (e.g., Liu et al. 1998). Such an instrument is able to

Corresponding author address: Dr. Gareth J. Marshall, British Antarctic Survey, High Cross, Madingly Road, Cambridge CB3 0ET, United Kingdom.
E-mail: gjma@pcmail.nbs.ac.uk

deduce directly both neutral stability wind speed and wind direction over the open ocean (scaled to a height of 10 m). Offiler (1994) stated that validation experiments indicated that ''the [ERS] scatterometer accuracy is about, or better than'' the nominal accuracies of 2 m s^{-1} (in the range of 4–24 m s^{-1}) and 20° for wind speed and direction, respectively. In addition, the spatial resolution of the ERS instrument is sufficiently small—50-km footprint resampled onto a 25-km grid—to enable it to detect mesoscale aspects of atmospheric flow. Dickinson and Brown (1996) showed that the scatterometer wind vectors were consistently able to reveal the storm fronts associated with marine cyclones, manifest as lines of wind shear. Furthermore, *ERS-1* scatterometer data have been used effectively in the study of Antarctic mesocyclones (Marshall and Turner 1997a; McMurdie et al. 1997) and coastal winds (Zecchetto and Bortoletto 1994; Marshall and Turner 1997b).

After providing a brief overview of how wind vectors over the ocean are derived using scatterometer instruments, this paper describes the ability of *ERS-1* scatterometer data to ''capture'' synoptic-scale (diameter exceeding 1000 km) systems over the Southern Ocean (SO). As a measure of success, the number of systems captured by the *ERS-1* scatterometer is compared to those contemporaneously observed in satellite imagery and/or present in weather charts using the number of cyclones existent during a month over a sector of the SO as a sample population. In addition, two case studies are used to illustrate the type of information regarding synoptic-scale weather systems that can be gleaned from scatterometer data—again comparing this to what can be derived from satellite imagery and/or is apparent on charts—and also to depict some of the problems that can occur with this type of data. First, a single swath containing several synoptic-scale features is described, and, second, an examination of three multitemporal swaths encompassing the same cyclone is undertaken. Finally, the utility of such data as an aid in the forecasting process over the data-sparse SO is considered.

2. ERS scatterometer winds

In this section a brief overview of the theory and problems behind scatterometer measurements of winds over the ocean is given. For a more comprehensive review see Thomas and Minnett (1986).

Assuming the energy transmitted back to a radar from the ocean is dependent only upon that component of sea surface roughness that is a product of the frictional interaction of wind on the surface (small-scale capillary waves), a model may be used to relate this roughness, through the radar backscatter coefficient, to wind speed and direction, the latter because the roughness is anisotropic with crests and troughs generally orthogonal to the wind direction. A generalized form of the backscatter coefficient σ^0 may be written as (Rees 1990)

$$\sigma^0 = aU^\gamma(1 + b\cos\psi + c\cos 2\psi), \qquad (1)$$

where U is the wind speed, ψ is the angle between the wind vector and the horizontal component of the scatterometer look direction, and a, b, c, and γ are constants dependent on frequency and incidence angle.

Once the wavelength of the capillary waves exceeds ~17.3 mm they become gravity waves (Kinsman 1965), whereby gravity, rather than surface tension, is the dominant restoring force. Gravity waves may cause problems with the basic model algorithm: certain developed sea conditions give rise to intermittent spikes in σ^0, and, because these conditions are controlled by the degree of wind–wave coupling, the backscatter is affected by nonlocal factors such as the wind fetch (Glazman et al. 1988). Additionally, sea surface temperature (Liu 1984) and atmospheric stability (Keller et al. 1985) can bias the wind speed model.

However, obtaining accurate wind speeds from scatterometer data has proved much less problematical than deriving wind direction. The ''harmonic'' nature of (1) necessitates the removal of a directional ambiguity, caused by the statistical properties of the sea surface being symmetrical about the wind direction. Theoretically, this may be achieved by measuring σ^0 at three different azimuth look angles. Thus, the ERS scatterometer has three sideways looking antennas that successively sweep over the same area at along-track nadir angles of +45°, 0°, and −45°, so for each point a set of backscatter ''triplets'' exist. The resultant possible directions are then weighted according to the deviation between the measured σ^0 values and those predicted by a backscatter model transfer function. The offline Institut Francais de Recherche pour l'Exploitation de la Mer (IFREMER) model function that has been utilized for processing the data illustrated in this paper is typical, in that the probability of the two most likely solutions—which are opposed—being correct is very similar, especially at low wind speeds and incidence angles (Quilfen 1995). One of these two solutions is correct in 98% of cases, so resolving the 180° upwind–downwind ambiguity is the principal potential error source with ERS scatterometer data (Quilfen and Cavanié 1991). This has led to the process of ''meteorological ambiguity removal'' whereby external wind field data are compared with the scatterometer data to decide the final ''correct'' solution. The offline IFREMER data use wind fields from European Centre for Medium-Range Weather Forecasts (ECMWF) analyses whereas forecast data are utilized when the scatterometer data are being assimilated into numerical analyses. Unfortunately, in the data-sparse SO the forecasts may sometimes not be sufficiently accurate; for example, if a closed synoptic depression is placed at the wrong location the forecast wind direction itself may be 180° in error. As part of the Antarctic First Regional Observing Study of the Troposphere (FROST) project, over 72 000 *ERS-1* scatterometer wind vectors were compared to collocated

(within 1.5 h) 75-m winds from the Australian Global Assimilation and Prediction (GASP) model, which does not use these data in real time: 3.4% of scatterometer winds were shown to have the directional ambiguity (Turner at al. 1996), which means that, in general, synoptic-scale systems can be easily recognized as such within scatterometer data but problems can remain with specific swaths, as illustrated by the case study described in section 6.

Another potential problem for determining the wind fields associated with synoptic systems in scatterometer data is the removal of local ambiguities using a field filter, a directional coherence test whereby the final direction chosen is partially dependent on those of the surrounding points. In initial processing algorithms this led to ''granularity'' whereby the wind direction was identical over extensive areas and then changed abruptly, totally unsuitable for portraying the changing wind directions around a depression center. To avoid directional errors propagating from ambiguities associated with low wind speeds, the IFREMER processing scheme does not dealias winds of less than 3 m s^{-1} (Quilfen 1995). In addition, sea ice is also detected to prevent the computation of fictitious winds over such regions (Gohin 1995).

3. Data and methodology

The dataset used in the study comprises *ERS-1* scatterometer wind vectors obtained during the month of January 1995. This was the third of three special observing periods (SOPs) that formed the FROST project (Turner et al. 1996), during which comprehensive datasets of model fields and in situ and satellite observations from Antarctica were obtained. The scatterometer data were processed using the IFREMER offline algorithm and made available to the British Antarctic Survey on CD-ROM, complete with software for efficiently interrogating the archive both temporally and spatially (Quilfen 1995). All the scatterometer swaths that were coincident with the spatial and temporal constraints of this study were produced as hardcopy output to ascertain whether any systems could be observed only in the scatterometer data.

In this study the scatterometer data are compared to both thermal infrared (TIR) Advanced Very High Resolution Radiometer (AVHRR) images—with a wavelength of 10.5–11.5 μm and a spatial resolution of 1 km—and the 12-h UKMO hand-drawn circumpolar SH charts, on which the centers of depressions are marked together with the location of fronts. The AVHRR imagery was obtained at the British Antarctic Survey's research station Rothera (67°34′S, 68°08′W), which has an acquisition mask radius of ~3000 km. Obviously, this places a limit on the region over which a comparison using the AVHRR imagery can be undertaken: the resultant region of interest for this study was defined as that between 50°–90°S and 10°–100°W (the south Atlantic–southeast Pacific sector). Note that the composite satellite images of the SH used by the UKMO in the construction of their charts also include AVHRR data in addition to that from geostationary satellites (Stearns et al. 1995). The AVHRR instrument is carried aboard the polar orbiting National Oceanographic and Atmosphere Administration (NOAA) satellites, and data from *NOAA-9, -10, -12* and *-14* were acquired during SOP-3.

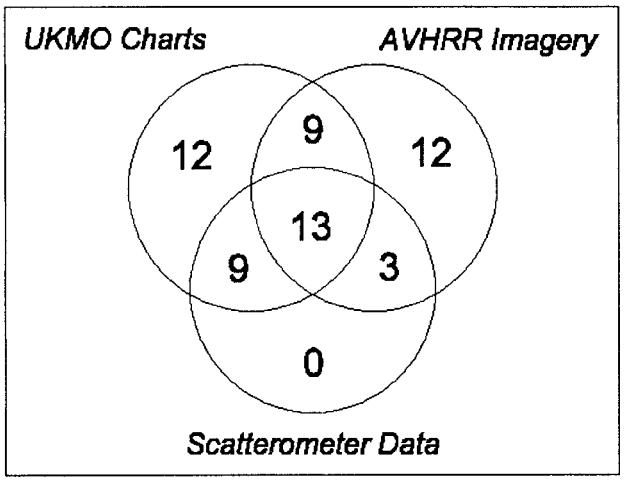

FIG. 1. Venn diagram summarizing the number of systems that could be observed in the UKMO charts, AVHRR imagery, scatterometer data, and various combinations of these. The total number of systems in the study dataset was 58.

The satellite imagery and charts were used to define the dataset for this work, that is, the number of synoptic systems that were present in the study region during January 1995. The duration of a system was calculated by rounding upward to the nearest half a day from the time between the first and last observations on a chart or satellite image, so that the minimum duration, including systems that were only observed once, was half a day.

4. The detection of synoptic-scale cyclones in the scatterometer data

For this study all systems having a diameter greater than 1000 km for at least part of their lifetime are included as synoptic scale. A cyclone's diameter is not necessarily easily defined because of the wide range of horizontal length scales demonstrated by SH systems. We define *cyclone diameter* as the distance across a system's cloud area exhibiting cyclonic curvature. Note that Turner et al. (1998) illustrate this definition in further detail using examples. A total of 58 synoptic-scale systems were present within the region of interest during the 31 days of SOP-3, and the numbers of systems that could be observed in the UKMO charts, AVHRR imagery, scatterometer data, and various combinations of these datasets are summarized in Fig. 1. Those 21 systems missing from the imagery were not coincident with

the NOAA satellite swaths during their lifespan. Although AVHRR data are incorporated into the composite satellite images used in the construction of the UKMO charts, both the spatial and radiometric resolution of the final product are significantly poorer than those of the Rothera AVHRR imagery. Turner et al. (1998) stated that the radiometric resolution is particularly important for identifying weather systems at high southern latitudes because many have associated cloud with a relatively featureless upper surface, making them hard to identify in the composite imagery. Thus, systems that appear distinct in the AVHRR imagery may not be present in the UKMO charts (15 systems in this study; cf. Fig. 1). Note that Fig. 1 also indicates that no systems were apparent only in the scatterometer data. Such a situation might arise if a synoptic system had a sufficiently featureless cloud signature to make it difficult to identify in the composite imagery while being coincident with a scatterometer swath but not an AVHRR swath. However, as the areal coverage of the AVHRR data is far superior to that of the scatterometer data—with two NOAA satellites each having an AVHRR swath approximately six times as wide as that of the *ERS-1* scatterometer—the numbers of systems involved would always be very small and indeed in this study was zero.

Eighteen of the 58 systems could not be observed by the scatterometer because they were located over sea ice, especially in the region of the Weddell Sea, and/or land for their entire existence in the study region during SOP-3. Of the remaining 40 systems, 25 were observed at least once by the scatterometer; that is, the combined effects of the spatial and temporal distribution of the narrow ERS scatterometer swath and missing data reduced the instrument's effectiveness in observing every synoptic system by ~38%. As expected, most of the missed systems were of short duration, with 10 of them lasting no more than half a day. However, one system that was missed had a duration of 3 days: missing scatterometer data was identified as the principal cause. Otherwise, all systems having a duration of 2 days or greater were successfully observed by the scatterometer. There were 43 scatterometer ''hits'' in total: the modal, median, mean, and maximum coverage per system were one, one, two, and six swaths, respectively.

The majority of the 25 SO systems studied had a single occluded front associated with them, but there were 11 where two separate fronts should, according to the near-coincident AVHRR imagery, be able to be discriminated in the scatterometer swaths. With the particular combination of the 43 scatterometer hits described previously the scatterometer data had the potential to capture 62 fronts during the study period. Of these, 47 (76%) could be discerned clearly, as a distinct kick in the wind vectors. Seven fronts (11%) could not be located because of granularity problems (cf. Fig. 3b) while in the remaining eight cases (13%) the wind vectors showed no indication of the front. For the latter systems, it is not clear whether the dealiasing algorithm failed or in fact these systems had a very weak surface circulation.

Marshall and Turner (1997a) demonstrated that the narrow data swath was the principal drawback in successfully capturing small-sized, short-lived Antarctic mesocyclones using ERS scatterometer data. However, synoptic systems are significantly larger in both diameter and life span and while the swath coverage remains a limitation in the observation of such weather systems, as noted by Brown and Zeng (1994), missing data are the most significant problem in this study. For the entire month of January 1995 the ratio of ERS scatterometer swaths crossing the study region that had missing data to those that did not was 1:2 but during the last third of the month there were considerably more data missing, and the ratio was 1:1. Quality assessment diagrams included on the IFREMER CD-ROMs show that the study region generally has a higher concentration of missing data than any other oceanic region. Often the cause is missing fore or aft beam data, resulting in data that are unable to be dealiased. However, the reason for the marked decline in the frequency of scatterometer data in the latter period of January can be linked directly to the operation of the ERS Advanced Microwave Instrument (AMI): the AMI comprises both the scatterometer and a synthetic aperture radar (SAR), and the use of the two instruments is mutually exclusive. There were no SAR images acquired in the study area prior to 16 January, but after this period there were typically between four and eight swaths per day when the SAR was switched on.

In addition, there were four scatterometer swaths that might have been expected to reveal a system but did not. Three of the systems that were associated with these swaths were successfully captured by the scatterometer data on another pass. In all four cases the cyclones were filling and the winds were light, leading to 180° directional ambiguity problems that were subsequently propagated along the swath.

5. Case study 1: Synoptic features observed in an *ERS-1* scatterometer swath

An *ERS-1* scatterometer swath passing through the study region and encompassing several synoptic-scale features is illustrated in Fig. 2a. These data were acquired between 1309 and 1315 UTC on 15 January 1995. For comparison, part of a TIR AVHRR image obtained at 1311 UTC (Fig. 2b) and the relevant section of the UKMO SH hand-drawn analysis for 1200 UTC (Fig. 2c) are shown. Three principal features may be observed in the scatterometer wind field.

Label A marks the center of a synoptic system located southwest of the Falkland Islands (centered at 54°S, 61°W), visible in the AVHRR image (Fig. 2b) because of the distinct comma cloud signature, but not readily apparent on the UKMO chart (Fig. 2c). Nonetheless, the

latter does indicate that it lay within a trough, a frequent location for cyclogenesis within the circumpolar trough (Turner et al. 1998). Farther south, the main axis of this trough can be observed in the scatterometer data as feature B. System A was first observed in the AVHRR imagery the previous day and appears to have formed immediately west of southern Chile. It then moved eastward at the leading edge of the trough until dissipating close to South Georgia (~55°S, 37°W) on 17 January. The cloud signatures suggest that the system was close to its maximum strength when the data in Fig. 2 were acquired.

Within the scatterometer wind field, the center of A is revealed by a specific wind field signature (Fig. 2a); wind speeds are greater (lower) on the equatorward (poleward) side of the center than the background flow, and the wind field shows troughing in an equatorward direction. Marshall and Turner (1997a) demonstrated that the wind fields associated with Antarctic *mesocyclones* (systems having a diameter less than 1000 km) could be explained using a simple model of a vorticity anomaly placed in a uniform flow. Using their classification, the system shown in Fig. 2a can be described as having *medium troughing*, the flow pattern most frequently observed in scatterometer data of Antarctic mesocyclones. For this type, the maximum wind speed of the anomaly is slightly less than that of the uniform flow (generally from a west by northwest direction in this example) so the resultant field has stronger winds on the equatorward side (wind fields of the background and anomaly are added) while the weaker winds on the poleward side (anomaly subtracted from background) have a similar direction to the background flow. All these features can be observed in Fig. 2a. There might be a manifestation of the granularity problem in a group of vectors (~25) on the eastern side of the swath immediately south of the 55°S parallel, where the winds change en masse from being northwesterly to northeasterly.

Feature B is that part of the trough running along a north-by-northwest–south-by-southeast axis (57°S, 66°W to 61°S, 63°W within the scatterometer swath). This feature can be observed clearly in the UKMO chart (Fig. 2c) in the shape of the 992-hPa isobar, but is not apparent from the cloud signatures in the AVHRR image (Fig. 2b). The scatterometer data (Fig. 2a) indicate that the wind-shear associated with the trough is marked, with the wind direction changing by up to 135° within the 25-km interval of the *ERS-1* scatterometer grid. This is not apparent in the UKMO chart (Fig. 2c) because of its lower spatial resolution and 4-hPa isobar interval. In Fig. 2b, a synoptic depression (C) can be seen dissipating in the ''cyclone graveyard'' of the Bellingshausen Sea (centered at 67°S, 72°W). The AVHRR image cloud signature is indicative of a weak circulation—disorganized but with some cloud elements still rotating—but no evidence of the low is shown on the UKMO chart. However, the contemporaneous scatterometer swath (Fig. 2a) reveals that the synoptic-scale low was still existent and had a weak but closed surface circulation, centered at 66°S, 72°W.

6. Case study 2: Multitemporal *ERS-1* scatterometer data of a Southern Ocean cyclone

This depression was initially identified on the UKMO charts at 0000, UTC 26 January, located at 55°S, 102°W, and first observed in an AVHRR pass acquired at 0533 UTC, when its center was at 57°S, 98°W. The low then followed a path typical of many systems entering the Bellingshausen Sea, spiraling in toward the southern Antarctic Peninsula, reaching its most easterly point of travel (69°S, 82°W) at ~1200 UTC 27 January. It then drifted slowly toward the southwest, following the coastline, and was last observed in the satellite imagery (2041 UTC 28 January) and synoptic charts (0000 UTC 29 January) at 74°S, 98°W and 69°S, 103°W, respectively, revealing a significant positional error in the charts. Such a large error in the location of a cyclone decaying in the Bellingshausen Sea in the UKMO charts was observed frequently, perhaps a consequence of the spatially ''confused,'' darker, lower-level cloud bands associated with cyclolysis being difficult to interpret in the 10-km resolution SH composites.

Analysis of the *ERS-1* scatterometer swaths indicates that four were coincident with the depression during its existence in the region of interest. Unfortunately, at the time of the last of these, on 28 January, one or more of the antennas was not operational south of ~55°S, so that the data in this region could not be dealiased. Sections of the other three scatterometer swaths are shown in Fig. 3.

The first of these was acquired at 1505 UTC 26 January (Fig. 3a) and shows the closed circulation associated with the cyclone center very clearly at 61°S, 93°W. The sharp turning of the winds east of the center is indicative of a front and the temporally closest AVHRR image, obtained less than an hour previously (1411 UTC; Fig. 4a), reveals that the frontal cloud band is in good spatial agreement with the front observed in the scatterometer field. A significant equatorward increase in velocity (from 5 to 20 m s^{-1}) is also apparent, as expected given the climatological westerly flow in the circumpolar trough.

In the second of the scatterometer passes (0622 UTC 27 January; Fig. 3b) the dealiasing algorithm failed badly: only some of the vectors have the correct direction with many showing an obvious 180° ambiguity. The center is probably located in the region having no vectors (i.e., low wind speeds) at 67°S, 89°W. Overall, the swath shows no evidence of the predicted closed circulation pattern. A contemporary AVHRR image (not shown) displays a similar cloud pattern to Fig. 4a, suggesting that the wind field was probably similar to that which the algorithm previously handled correctly. One possible reason for the problem is the linear disruption

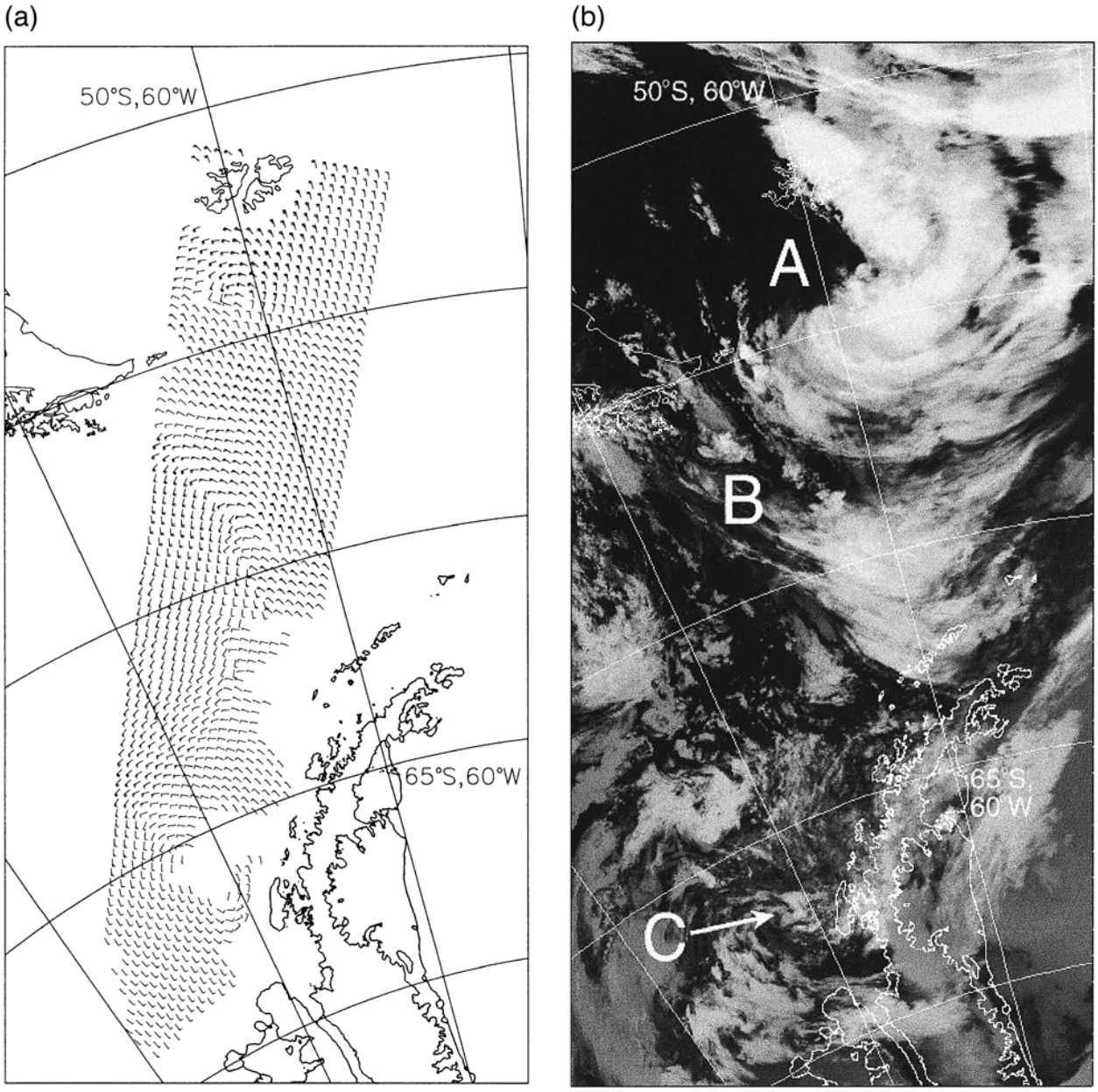

FIG. 2. Near-coincident data over the Southern Ocean on 15 Jan 1995. (a) *ERS-1* scatterometer swath acquired between 1309 and 1315 UTC; (b) TIR AVHRR imagery obtained at 1311 UTC; (c) UKMO Southern Hemisphere hand-drawn analysis for 1200 UTC. Wind feathers point in the direction the wind is blowing; half a barb denotes 2.5 m s^{-1}, and a full barb 5.0 ms^{-1}. The three features labeled in (b) and (c) are discussed in the text. Note that the latitude and longitude intervals are 5° and 10°, respectively.

at the southern end of the swath caused by missing data. Thus, even when a swath is coincident with a depression, there may still be problems identifying it solely from its wind field as an automatic detection algorithm might attempt to do.

The nonlinear disruption at the southern end of the third swath (1435 UTC 27 January; Fig. 3c) is indicative of the sea ice edge. The wind vectors suggest that the center of the depression lies just south of the edge at this time at 68°S, 89°W. Near-coincident AVHRR imagery (1358 UTC; Fig. 4b) shows that the system was undergoing cyclolysis (dissipating), with disorganized cloud bands and no clear center. The maximum wind velocity had declined to ~10 m s^{-1}.

7. The utility of scatterometer data in forecasting

The surface wind vectors derived from scatterometer instruments appear to be a potentially valuable form of data in supplementing the very few observations that

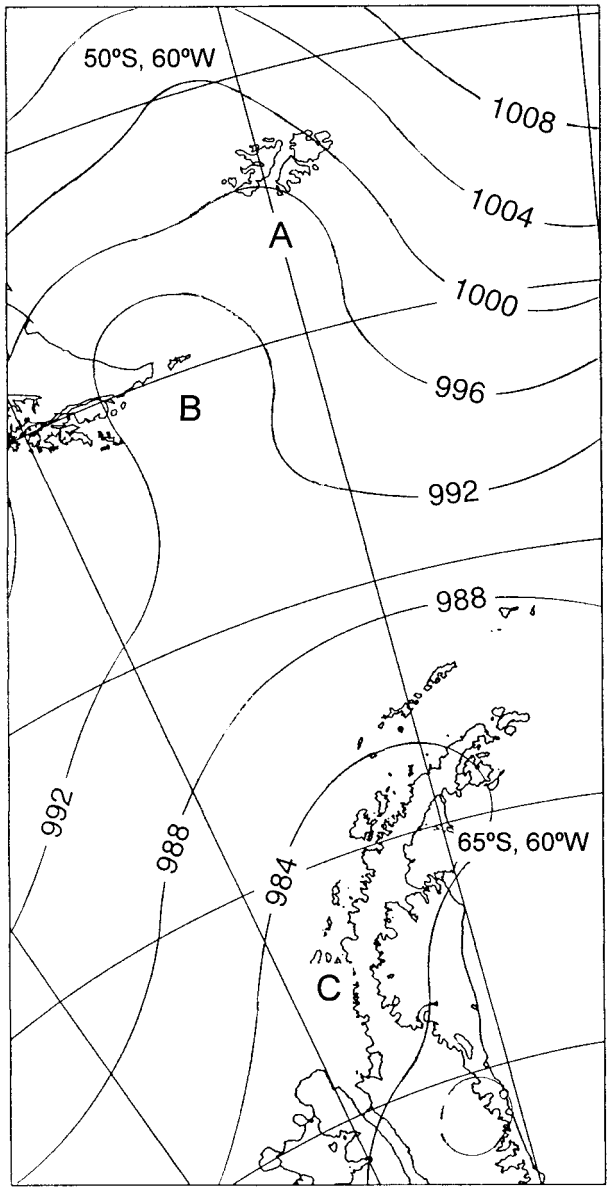

FIG. 2. (*Continued*)

are available over the SO. Bell (1994) stated that over the SH oceanic region as a whole the scatterometer provided 100 times more wind speed data than did ship reports, and this figure will obviously be even greater over the especially data-sparse SO. As far as meteorological analysis is concerned, there are two main applications of the vectors: use of the observations in the preparation of manual analyses and the direct assimilation of the vectors into numerical analysis schemes.

Today, hand-drawn surface analyses are still prepared in a number of forecast offices as part of the process of verifying the numerical analyses and the observational dataset. Incorrect or suspect observations can be detected and then corrected prior to their incorporation within the assimilation scheme or rejected outright. The scatterometer winds allow the direction of the surface flow to be analyzed accurately and also provide a useful proxy indication of the surface pressure gradient in regions where no observations exist. When significant differences are found between the manual and computer analyses, then ''bogus'' or pseudo-observations can be generated and utilized in subsequent runs of the assimilation scheme to improve the representation of certain synoptic features. The highest spatial resolution used in the current generation of global NWP models is ~80 km. Therefore, the higher resolution of the scatterometer data can potentially resolve features that are unable to be represented correctly in the numerical analyses (e.g., Liu et al. 1998). Features such as polar mesocyclones, narrow zones of convergence, and frontal bands can all be important for forecasting but may be misrepresented or indeed not represented at all in current computer analyses. Careful manual analysis of the scatterometer data can therefore be of significant benefit in some forecasting situations. For example, the wind vectors allow the positions of cyclones to be determined accurately and provide an accurate reflection of their vigor. Moreover, Brown and Zeng (1994) were able to estimate the central pressures of cyclones by using ERS winds as a boundary condition in a planetary boundary layer model, from which the pressure gradients could be calculated and subsequently calibrated using a point pressure outside the region of the storm. These authors found that the pressures derived from the scatterometer–model data were generally 2 mb less than that in the ECMWF analyses; however, as the latter were used to calibrate the former, the method demonstrated the ability to define storm details (i.e., location of fronts) rather than absolute pressures. Nonetheless, as the spatial resolution of NWP models is too coarse for accurately identifying the intensity of a system and the use of schemes based on cloud features in satellite imagery is somewhat subjective, an objective method as advanced by Brown and Zeng (1994) could prove invaluable in forecasting. Other useful parameters for studying cyclones are the cyclonic relative vorticity and divergence, and the unique capability of the scatterometer instrument to obtain both wind speed and direction enables the derivation of such differential motion parameters (e.g., Long 1993; Marshall and Turner 1997a; McMurdie et al. 1987).

Scatterometer data have been regularly assimilated into NWP models since 1993–94 and details of how this is achieved in the UKMO and ECMWF analysis and forecasting systems are given by Bell (1994) and Stoffelen et al. (1994), respectively. Note that both assimilation schemes do the final ambiguity removal in-house, with the UKMO incorporating the original backscatter data while the ECMWF scheme takes pairs of dealiased upwind–downwind wind vectors. The significantly higher resolution of the scatterometer data as compared to the model resolution means that they are necessarily thinned at some point. In the ECMWF scheme the wind

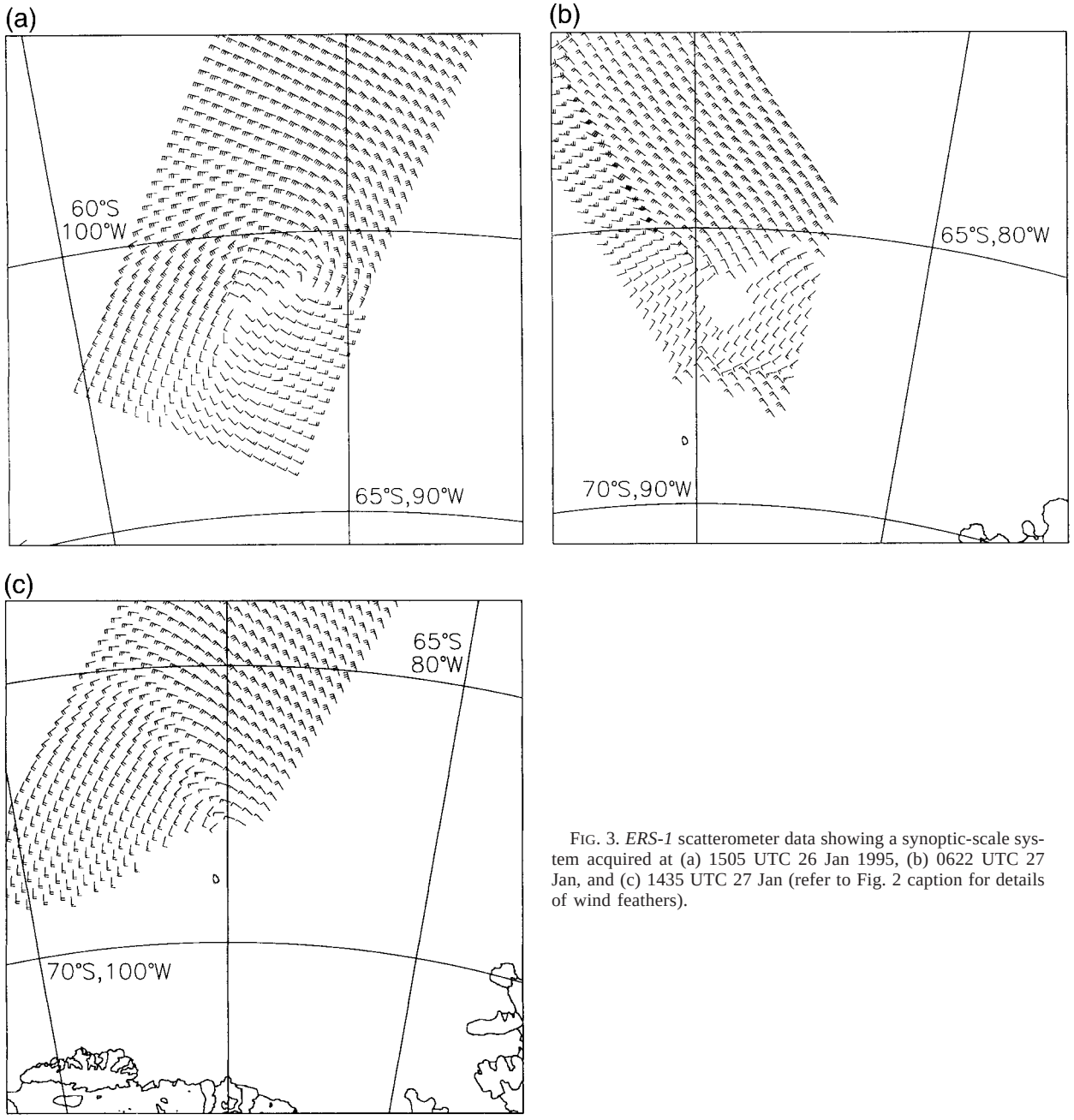

FIG. 3. *ERS-1* scatterometer data showing a synoptic-scale system acquired at (a) 1505 UTC 26 Jan 1995, (b) 0622 UTC 27 Jan, and (c) 1435 UTC 27 Jan (refer to Fig. 2 caption for details of wind feathers).

vectors are thinned to 100 km prior to assimilation (Gaffard and Roquet 1995), while in the UKMO all observations are assimilated and a different subset (a fifth of the data) is used for each analysis iteration, thus avoiding problems of bias associated with preliminary averaging of the data (Bell 1994). Both systems also include further quality control steps to those provided in the original data; for example, the ECMWF scheme makes use of SST operational analyses to reject wind vectors when there is a chance of sea ice contamination (SST < 0°C), above the seawater freezing point to allow for errors in the SSTs (Gaffard and Roquet 1995).

Two studies on the effect of assimilating ERS scatterometer data into NWP forecast models over the SH have indicated that their overall impact is neutral. Hoffman (1993) used an early version of the scatterometer model transfer function in conjunction with the ECMWF system. He examined four forecasts in the SH: of these, in one the scatterometer data had a positive effect, in one negative, and in two neutral. Differences arose from small quasi-random perturbations that propagated in subsequent forecasts. Jacka (1997) utilized the more advanced CMOD4 model transfer function in his analysis based on the Australian Bureau of Meteorology

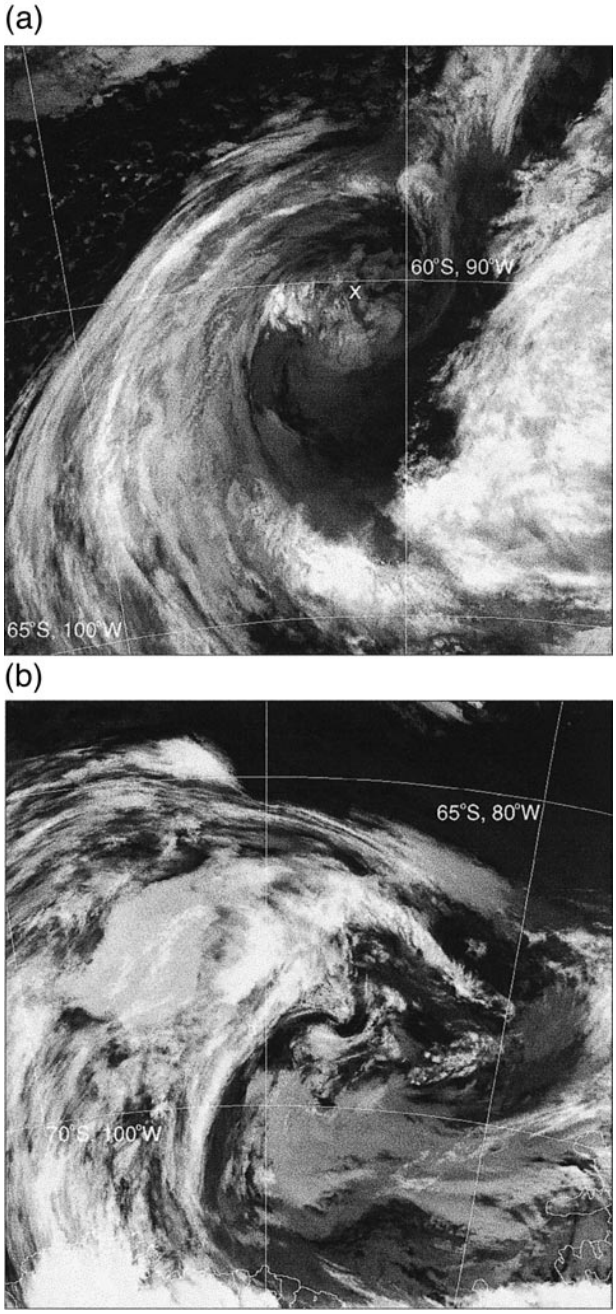

FIG. 4. *TIR* AVHRR imagery of a synoptic-scale system acquired at (a) 1411 UTC 26 Jan 1995 and (b) 1358 UTC 27 Jan.

GASP system for the month of July 1995. Several individual cases with analysis impacts of 10–15 hPa were identified. These events resulted directly from an alteration of quality control decisions caused by the scatterometer data supporting or refuting MSLP data from buoys or ships. Again, the mean impact over the whole month was effectively neutral.

However, other studies have demonstrated clear positive impacts of assimilating ERS scatterometer data into forecasts over the SH. Bell (1994) showed that in the UKMO operational analyses the effect of assimilating scatterometer data gave substantial (10%) reductions in the rms errors (between forecast and observations) for the surface and low-level height at all forecast ranges with additional smaller reductions in temperature and wind rms errors. A study by Gaffard and Roquet (1995), analyzing the impact of ERS scatterometer data on the ECMWF 3D-Var assimilation scheme in terms of 1000-hPa geopotential, demonstrated that the influence of the scatterometer data for short-range (12 h) forecasts was ''positive or neutral almost everywhere in the SH,'' with the biggest impact over the SO and northeast of New Zealand (cf. their Fig. 10a). For medium-range (48 h) forecasts the effect was more neutral.

Scatterometer winds from the ERS satellites do have some problems that must be borne in mind when they are being used in an operational environment. One of the most frustrating problems is that vectors cannot be produced if the wind speed is greater than 24 m s^{-1}—due to saturation of the radar returns when the sea is very rough—which cannot be circumvented. This is particularly unfortunate since forecasters need to know the wind speeds associated with rapidly deepening lows, which, over the SO, occur preferentially near 45°–50°S in the South Indian and Atlantic Oceans (Sinclair 1995). The problem of not being able to derive winds at very low speeds is less significant although it will make the estimation of the center of a low more difficult.

For manual analysis, vectors with the 180° directional ambiguity can be detected fairly easily by an experienced analyst. However, although the problem of granularity, whereby a field of nearly identical vectors is returned over a large part of the swath, is not frequently observed in the IFREMER data, it does present problems for a manual analysis when it is present. In addition to showing directional problems in the resolved vectors, Fig. 3b also reveals evidence of granularity: instead of a slowly varying field of vectors around the center of a low, the wind field appears as a number of blocks of data, where the winds in each block have an identical direction. With such data it is very difficult to determine where fronts are located and wholly spurious lines of convergence or divergence may be identified.

The use of meteorological ambiguity removal techniques as part of the process to decide the wind direction (see section 2) must be considered; as with any scatterometer winds assimilated into the numerical analysis scheme, they will not be truly independent and the full value of the data may not be realized. Further problems may be experienced when a small vortex is not represented in the numerical analysis but is present in the scatterometer data; this situation occurred three times in this study (cf. Fig. 1). In such cases the model fields cannot help in the ambiguity removal and a large number of vectors may be 180° in error. On occasions such as this, when a feature is not resolved by the model fields, the scatterometer data have the greatest potential

to be of benefit and improve the forecasts. Additional research needs to be undertaken into how the scatterometer data can help improve the numerical analyses, particularly when the models and satellite data present conflicting views of a situation.

8. Conclusions

Using data obtained during the third FROST SOP, we have attempted to show that wind vectors over the ocean surface derived from spaceborne scatterometer instruments provide a useful tool for observing synoptic-scale features, and that other studies have revealed that this type of data has a role to play in the forecasting process over the data-sparse SO, where they may well be the only type of observation available. For manual analysis the 25-km grid of the ERS data allows an improved location of cyclone centers compared with the numerical analysis schemes. In addition, fronts may usually be delineated precisely and were found to match accurately frontal cloud bands observed in contemporaneous TIR imagery. One problem with the data is the narrow swath, which means that some relatively short-lived systems may be missed. However, for systems existent for at least 24 h, particularly those at high latitudes where orbital coverage improves due to overlapping swaths, it is highly probable that they will be captured within a scatterometer swath at least once during their lifetime. Multitemporal data—typically each system was observed twice—allow an examination of cyclone development through the calculation of changes in wind velocity and relative vorticity.

This study has also highlighted two significant limitations regarding the use of ERS scatterometer data for observing synoptic weather systems over the SO. First, the range of winds for which vectors may be derived is constrained at both ends of the scale: strong winds associated with rapidly deepening lows approaching Antarctica cannot be determined, while the poor accuracy of wind directions at low wind speeds means that the wind fields associated with dissipating cyclones may be incorrect. Second, the ERS scatterometer cannot be used when the SAR is switched on, resulting in a high potential loss of data when this instrument is switched on prior to reaching the sea-ice edge or Antarctic continent. A more minor difficulty results from the continuing problem of granularity in a limited number of cases.

Acknowledgments. The authors would like to acknowledge the help of the IFREMER staff at the French ERS PAF involved with disseminating the offline scatterometer products.

REFERENCES

Bell, R. S., 1994: Operational use of ERS-1 products in the Meteorological Office. *Proc. Second ERS-1 Symp.: Space at the Service of our Environment,* Vol. 1, Hamburg, Germany, European Space Agency, 195–200.

Brown, R. A., and L. Zeng, 1994: Estimating central pressures of oceanic midlatitude cyclones. *J. Appl. Meteor.,* **33,** 1088–1095.

Dickinson, S., and R. A. Brown, 1996: A study of near-surface winds in marine cyclones using multiple satellite sensors. *J. Appl. Meteor.,* **35,** 769–781.

Gaffard, C., and H. Roquet, 1995: Impact of the ERS-1 scatterometer wind data on the ECMWF 3D-Var assimilation system. ECMWF Research Department Tech. Memo. 217, 21 pp. [Available from European Centre for Medium-Range Weather Forecasts, Shinfield Park, Reading RG2 9AX, United Kingdom.]

Glazman, R. E., G. G. Pihos, and J. Ip, 1988: Scatterometer wind speed bias induced by the large-scale component of the wave field. *J. Geophys. Res.,* **93,** 1317–1328.

Gohin, F., 1995: Some active and passive microwave signatures of Antarctic sea ice from midwinter to spring 1991. *Int. J. Remote Sens.,* **16,** 2031–2054.

Guymer, T. H., 1983: A review of Seasat scatterometer data. *Philos. Trans. Roy. Soc. London,* **309A,** 399–414.

Hoffman, R. N., 1993: A preliminary study of the impact of the ERS 1 C band scatterometer wind data on the European Centre for Medium-range Weather Forecasts global data assimilation scheme. *J. Geophys. Res.,* **98,** 10 233–10 244.

Ingleby, N. B., and R. A. Bromley, 1991: A diagnostic study of the impact of SEASAT scatterometer winds on numerical weather prediction. *Mon. Wea. Rev.,* **119,** 84–103.

Jacka, K. J., 1997: Impact of ERS-1 scatterometer wind data in the Australian Bureau of Meteorology Global Assimilation and Prediction system. Preprints, *Fifth Int. Conf. on Southern Hemisphere Meteorology and Oceanography,* Pretoria, South Africa, Amer. Meteor. Soc., 41–42.

Katsaros, K. B., and R. A. Brown, 1991: Legacy of the Seasat mission for studies of the atmosphere and air–sea–ice interactions. *Bull. Amer. Meteor. Soc.,* **72,** 967–981.

Keller, W. C., W. J. Plant, and D. E. Weissman, 1985: The dependence of X band microwave sea return on atmospheric stability and sea state. *J. Geophys. Res.,* **90,** 1019–1029.

Kinsman, B., 1965: *Wind Waves—Their Generation and Propagation on the Ocean Surface.* Prentice-Hall, 676 pp.

Levy, G., and R. A. Brown, 1991: Southern Hemisphere synoptic weather from a satellite scatterometer. *Mon. Wea. Rev.,* **119,** 2803–2813.

Liu, W. T., 1984: The effects of the variation in sea surface temperature and atmospheric stability in the estimation of average wind speed by SEASAT-SASS. *J. Phys. Oceanogr.,* **14,** 392–401.

——, W. Tang, and P. S. Polito, 1998: NASA scatterometer provides global ocean-surface wind fields with more structures than numerical weather prediction. *Geophys. Res. Lett.,* **25,** 761–764.

Long, D. G., 1993: Wind field model-based estimation of Seasat scatterometer winds. *J. Geophys. Res.,* **98,** 14 651–14 668.

Marshall, G. J., and J. Turner, 1997a: Surface wind fields of Antarctic mesocyclones derived from ERS-1 scatterometer data. *J. Geophys. Res.,* **102** (D12), 13 907–13 921.

——, and ——, 1997b: Katabatic wind propagation over the western Ross Sea observed using ERS-1 scatterometer data. *Ant. Sci.,* **9,** 221–226.

McMurdie, L. A., G. Levy, and K. B. Katsaros, 1987: On the relationship between scatterometer-derived convergences and atmospheric moisture. *Mon. Wea. Rev.,* **115,** 1281–1294.

——, C. Claud, and S. Atakturk, 1997: Satellite-derived atmospheric characteristics of spiral and comma-shaped Southern Hemisphere mesocyclones. *J. Geophys. Res.,* **102,** 13 889–13 905.

Offiler, D., 1994: The calibration of *ERS-1* satellite scatterometer winds. *J. Atmos. Oceanic Technol.,* **11,** 1002–1016.

Quilfen, Y., 1995: ERS-1 off-line wind scatterometer products. Centre ERS d'Archivage et de Traitement Rep. C1-EX-MUT-CD0000-03-IF, version 1.1, 58 pp. [Available from IFREMER-CERSAT, BP 70, 29280 Plouzané, France.]

——, and A. Cavanié, 1991: A precision wind algorithm for the ERS1 scatterometer and its validation. *Proc. IGARSS 91, Remote Sens-*

ing: Global Monitoring for Earth Management, Espoo, Finland, IEEE, 873–876.

Rees, W. G., 1990: *Physical Principles of Remote Sensing.* Cambridge University Press, 247 pp.

Sinclair, M. R., 1995: A climatology of cyclogenesis for the Southern Hemisphere. *Mon. Wea. Rev.*, **123,** 1601–1619.

Stearns, C. R., J. T. Young, and B. Sinkula. 1995: Two years of IR images south of 40°S every three hours. Preprints, *Fourth Conf. on Polar Meteorology and Oceanography*, Dallas, TX, Amer. Meteor. Soc., 112.

Stoffelen, A., C. Gaffard, and D. Anderson, 1994: ERS-1 scatterometer data assimilation. *Proc. Second ERS-1 Symp.: Space at the Service of our Environment*, Vol. 1, Hamburg, Germany, European Space Agency, 191–194.

Thomas, I. L., and P. J. Minnett, 1986: An introductory review of the measurement of ocean surface wind vectors with a satellite radar scatterometer. *Int. J. Remote Sens.*, **7,** 309–323.

Turner, J., and Coauthors, 1996: The Antarctic First Regional Observing Study of the Troposphere (FROST) project. *Bull. Amer. Meteor. Soc.*, **77,** 2007–2032.

——, G. J. Marshall, and T. Lachlan-Cope, 1998: A satellite-derived climatology of synoptic-scale low pressure systems within the Antarctic peninsula sector of the circumpolar trough. *Int. J. Climatol.*, **18,** 253–280.

Zecchetto, S., and M. Bortoletto, 1994: Examples of mesoscale meteorology in the Mediterranean Sea using ERS-1 scatterometer data. *Proc. Second ERS-1 Symp.: Space at the Service of our Environment*, Vol. 2, Hamburg, Germany, European Space Agency, 815–818.